RSC Advances

ROYAL SOCIETY OF CHEMISTRY

www.rsc.org/advances

RSC Advances

RSCPublishing

ARTICLE

Is Cu_3SbSe_3 a promising thermoelectric material?†

Cite this: DOI: 10.1039/xoxxoooooox

Tian-Ran Wei, Chao-Feng Wu, Wei Sun, Yu Pan and Jing-Feng Li*

Received ooth January 2012,
Accepted ooth January 2012

DOI: 10.1039/xoxxoooooox

www.rsc.org/

Cu_3SbSe_3, a compound with an ultralow thermal conductivity, has been predicted as a promising thermoelectric material, but relevant experimental results are inadequate. In this work we studied the high-temperature thermoelectric properties of this ternary chalcogenide. Extremely low thermal conductivity was observed and a glass-like behavior was seen above an order-disorder transition. Possible mechanisms causing such an ultralow thermal conductivity were discussed concerning the disorder of Cu atoms. With a large band gap of ~0.95 eV obtained by optical absorption edge measurement, Cu_3SbSe_3 was found to be a nondegenerate p-type semiconductor, different from previous reports. Maximum zT of ~0.25 was obtained at 650 K for Cu_3SbSe_3, which is much higher than previously reported values, but this compound was considered inferior to Cu_3SbSe_4 in thermoelectric performance by comparing some key physical parameters.

Introduction

Thermoelectric (TE) technology has drawn wide attention over the past two decades mainly because of its applicability for direct conversion from waste heat to electricity, which is expected to provide one solution for the global energy and environmental problems.[1,2] The efficiency of TE conversion is mostly determined by the materials' dimensionless figure of merit, $zT=S^2T/\rho\kappa$, where S, T, ρ and κ are Seebeck coefficient, absolute temperature, electrical resistivity and thermal conductivity, respectively.[3-5] Currently Bi_2Te_3- and PbTe-based alloys are the state-of-the-art TE materials for low and middle temperature applications, but they contain the scarce Te, bringing about serious concerns on sustainable use. Consequentially searching for and developing high-performance TE materials free of Te has become a popular trend in this field.[6,7] Among these candidates, many binary and multinary selenides with low κ have been found to exhibit promising zT values, such as the layered oxide BiCuSeO,[8,9] liquid-like $Cu_{2-x}Se$[10,11] and the recently reported SnSe.[12,13]

Being composed of earth-abundant elements, Cu-Sb-Se ternary selenides, belonging to the vast Cu-M-Ch (M=IIIA, IVA and VA elements and Ch=S, Se and Te) group with a diamond-like tetrahedral structure, have also attracted interests in the field of thermoelectricity. In fact, zT about unity has been obtained in Cu_3SbSe_4,[14,15] and $Cu_{12}Sb_4Se_{13}$ was also theoretically predicted to be a new promising TE material.[16] Cu_3SbSe_3 was found to exhibit an ultralow thermal conductivity characterized by a large lattice anharmonicity[17] that was thought to be governed by the lone-pair electrons of Sb[18] and the "part-crystalline part liquid state".[19] Partly because of the intriguingly low κ, Cu_3SbSe_3 was considered to be a promising TE material,[20] but experimental results on this issue are severely inadequate, in contrast to the widely studied Cu_3SbSe_4,[21,22] possibly because of the difficulty in obtaining single-phased samples.[23] Up until recently, Tyagi *et al.*[24,25] reported TE properties of Cu_3SbSe_3 for the first time according to our knowledge. In those reports Cu_3SbSe_3 samples fabricated *via* the solid-state reaction followed by spark plasma sintering (SPS) exhibited a metallic behavior in electrical transport despite a large band gap[20,26] and achieved a relatively low zT<0.1.

With interest in the ultralow thermal conductivity, the predicted but rarely confirmed TE potential and the surprising electrical properties by the previous studies, we prepared polycrystalline Cu_3SbSe_3 compounds *via* different methods and studied the TE properties in the range of 300-650 K. Studying the properties of samples prepared by different methods will provide a more convincing evaluation of intrinsic properties of this compound. Cu_3SbSe_3 in this work was found to exhibit an extremely low κ and behave as a typically nondegenerate semiconductor with the highest zT of 0.25 being obtained at 650 K, which is much higher than previously reported values. A comparison of Cu_3SbSe_3 with Cu_3SbSe_4 was demonstrated concerning some physical parameters, giving an insight into the difference in TE performance between the two compounds with similar chemical composition.

Experimental

Stoichiometric Cu, Sb and Se raw powders were mixed and sealed into quartz tubes that were evacuated and slowly heated up to 1273 K, soaked for 12 h and then quenched in water, followed by annealing at 623 K for 5 days. The obtained ingots were pulverized and densified by hot pressing (HP) at 673 K for 1 h under 50 MPa in Ar. Samples fabricated by this method are donated as Q-A-HP. For comparison, Cu_3SbSe_3 were also synthesized by mechanical alloying (MA), for which raw powders were milled using a planetary ball mill at 450 rpm for 15 h in a stainless steel vessel filled with 95 vol% Ar and 5 vol% H_2 gases, followed by HP as described for Q-A-HP. Samples obtained *via* this method are donated as MA-HP. Some of the MA-HP samples were annealed at 623 K in evacuated quartz tubes for 24 h, donated as MA-HP-A.

The phase purity of the samples were investigated by using X-ray diffraction (XRD, RINT2000, Rigaku, Japan) equipped with Cu K_α radiation. Rietveld refinement was carried out to calculate the lattice parameters. Morphologies of fractured and polished surfaces were observed by scanning electron microscopy (SEM, JSM-7001, JEOL, Japan). Microstructures as well as grain morphologies were further investigated by using the transmission electron microscopy (TEM, 2011, JOEL, Japan). Electronic probe microscopic analysis (EPMA, JXA-8230, JEOL, Japan) was used to analyze the ratio and distribution of the elements on polished surfaces of bulk samples. Seebeck coefficient (S) and electrical resistivity (ρ) as functions of temperature were measured using a Seebeck coefficient/electric resistance measuring system (ZEM-2, Ulvac-Riko, Japan). Hall coefficient (R_H) at room and high temperatures was measured under a reversible magnetic field of 0.52 T by the Van der Pauw technique using a Hall measurement system (ResiTest 8340DC, Toyo, Japan). The Hall carrier concentration (n_H) was calculated *via* $n_H=1/(eR_H)$, and the Hall carrier mobility (μ_H) was obtained through $\mu_H=R_H/\rho$. The thermal diffusivity (D) was measured using a laser flash diffusivity method (TC9000, Ulvac-Riko, Japan). The specific heat capacity (C_P) as well as the melting point was measured by the Differential Scanning Calibrator (DSC, STA449F3, Netzsch, Germany). Thermal conductivity (κ) was calculated by $\kappa=DC_Pd$, where d is the density measured by the Archimedes method. Electrical and thermal properties were measured at least twice for all the samples. Measurement repeatability and discussions on samples' thermal stability can be found in the electronic supplementary information (†ESI). Optical absorption edge measurement was conducted on powder samples by using the UV-Vis-NIR spectrum (Cary 5000, Varian, America) at room temperature. The optical gaps were obtained by extrapolating $(\alpha hv)^n$ to 0 as a function of hv (where α is the absorption coefficient, hv is the photon energy, and n is equal to 2 for direct gaps, 0.5 for indirect gaps).

Results and discussion

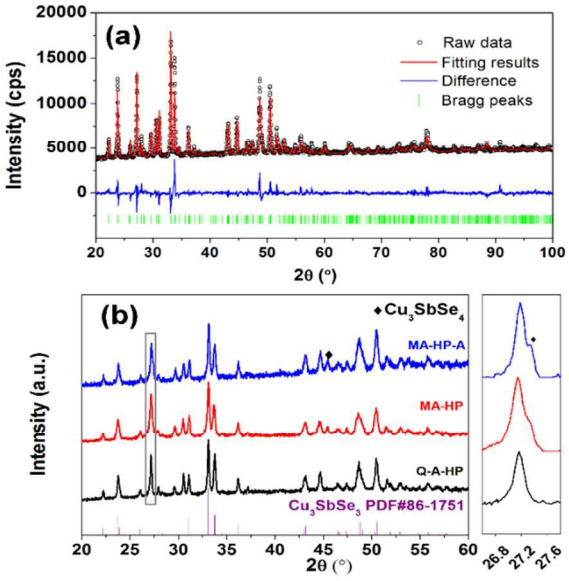

Fig.1 (a) Powder XRD data of Cu_3SbSe_3 prepared by melting, quenching and annealing with Rietveld refinement results. (b) XRD patterns of bulks fabricated by different methods.

Figure 1 (a) demonstrates the powder XRD patterns of Cu_3SbSe_3 obtained by melting, quenching and annealing. The Rietveld refinement data indicates a single phase crystallized in an orthorhombic structure of the Pnma space group with lattice constants a=7.9811 Å, b=10.6044 Å and c=6.8337 Å, consistent with Pfitzner's data.[27] This result indicates high phase purity of samples prepared by quenching, annealing and hot pressing. For bulks, as shown in Fig. 1 (b), the sample Q-A-HP, densified from the above powders shows a single phase of Cu_3SbSe_3, while MA-HP and MA-HP-A contain small amount of Cu_3SbSe_4. It is noted that in a previous report, different secondary phases of $CuSbSe_2$ and Cu_2Se were found in preparing Cu_3SbSe_3 by a similar melting, quenching and annealing method.[23]

Table 1 Density and chemical composition of Cu_3SbSe_3 samples.

Samples' label	Density (g/cm^3)	EPMA atomic ratio Cu:Sb:Se
Q-A-HP	5.56	45.0: 14.4: 40.6
MA-HP	6.12	44.7: 14.5: 40.8
MA-HP-A	4.94	43.6: 14.8: 41.6

The sample Q-A-HP shows a typically ingot-like polished surface morphology with a homogenous elemental distribution as demonstrated in Fig. 2 (a). MA-HP exhibits a dense microstructure with grain sizes of 100-300 nm as shown by the SEM [Fig. 2(b)] and TEM [Fig. 2(c)] images. MA-HP-A, subjected to a long annealing process, has a porous feature corresponding to a low density [Fig. 2 (d)]. Samples' density and chemical composition are listed in Table 1. Elemental ratio Cu:Sb:Se of the samples is close to the nominal one 42.9:14.2:42.9 despite small deviation that might be caused by Se volatilization during fabrication process.

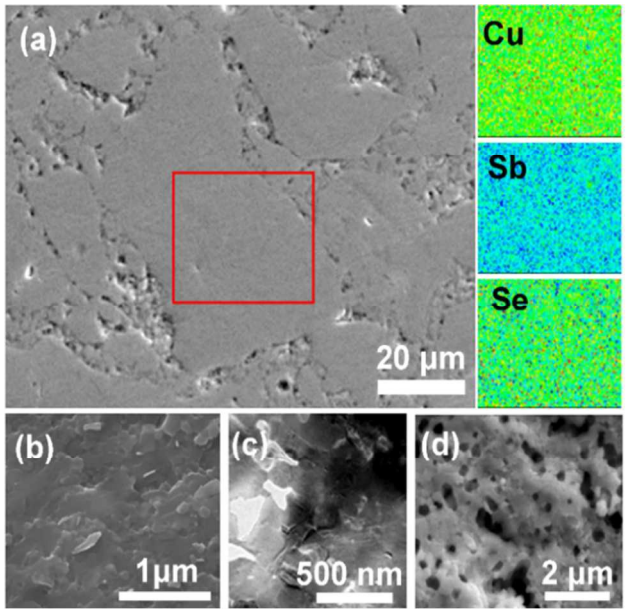

Fig. 2 (a) SEM image of the polished surface of Q-A-HP with elemental distribution in the red rectangle by EPMA, (b) SEM image of the fractured surface for MA-HP, (c) grains' morphology of MA-HP by TEM and (d) fractured surface morphology of MA-HP-A by SEM.

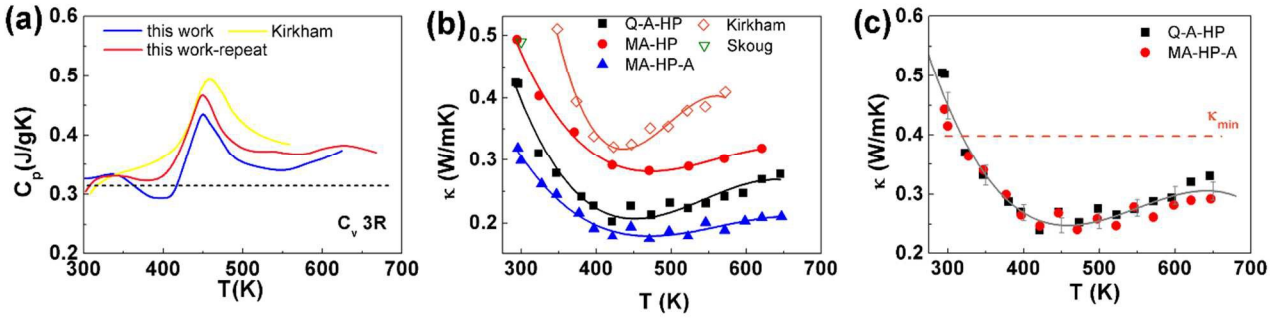

Fig. 3 (a) C_P and (b) κ of Cu_3SbSe_3 as functions of temperature with reported values by Skoug (ref. 18) and Kirkham (ref. 23), (c) κ of "fully dense" Cu_3SbSe_3 with κ_{min} for reference. Solid curves in (b) and (c) are added to guide the eyes. Error bars in (c) represents 5 % measurement uncertainty.

C_P is shown in Fig. 3(a) together with the reported value from ref. 23. A well-defined peak at 450 K is observed, which was ascribed to the order-disorder transition of Cu atoms.[23,28] This transition has been confirmed by Kirkham *et al.*[23] *via* high-temperature XRD where a nonlinear thermal expansion behavior is seen between 398 and 448 K and charge flipping analysis indicates that Cu atoms become disordered above the transition temperature. The disorder behavior of Cu atoms is expected to intensify phonon scattering. In almost the whole measurement temperature range C_P is larger than the Dulong-Petit limit. It is different from the case of liquid-like Cu atoms in $Cu_{2-x}Se$ where C_P is considerably smaller than the limit caused by the absence or suppression of transverse mode in phonon propagation.[10] This difference suggests that the fluidity of Cu atoms in Cu_3SbSe_3, should there be, would not be remarkable enough to significantly hinder the propagation of shear modes as the case in $Cu_{2-x}Se$. Another supportive evidence for this argument is that Cu atoms in Cu_3SbSe_3 are tetrahedrally bonded making it hard to freely move, while Cu in $Cu_{2-x}Se$ distribute in and freely travel among the large space of the interstitial sites of the Se fcc sublattice.[10]

κ of Cu_3SbSe_3 is shown in Fig. 3 (b) with previous reported values by Skoug[18] and Kirkham.[23] From electrical conductivity measurements (to be shown later), the electronic component κ_e contributed <3% to the total κ, so here the lattice component κ_L was treated numerically equal to κ. κ first decreases to a minimum value around 450 K and then slowly increases at higher temperatures. Thermal transport at T>450 K is a typical behavior of amorphous solids.[29] For amorphous solids (glasses), the scattering of phonons is so intense that their mean free paths (MFPs) are limited to the order of atomic distances and cannot be further reduced. According to the relationship of $\kappa=1/3Cvl$ (where C, v and l are heat capacity per unit volume, sound speed and MFPs of phonons),[30] κ will increase with the rise of heat capacity.

In order to remove the effect of porosity and attain a reasonable comparison with different materials, the values thermal conductivity (κ) were extrapolated to the 100% dense case (κ_{dense}) by the relation

$$\frac{\kappa}{\kappa_{dense}} = 1 - \frac{4}{3}\phi, \qquad (1)$$

where ϕ is the porosity.[31] It is found that κ normalized from Q-A-HP and MA-HP-A yield a reasonably similar value [see Fig. 3 (c)], partly consolidating the relation. The minimum thermal conductivity κ_{min} was estimated to be about 0.4 W/mK using the Cahill's formula at the high-temperature limit[30,32]

$$\kappa_{\min} = \frac{1}{2}\left(\frac{\pi}{6}\right)^{1/3} k_B n^{2/3}(2v_t + v_l), \qquad (2)$$

where n is the number of atoms per unit volume, and v_t, v_l are the transverse and longitudinal sound speeds, respectively, whose values were taken from ref. 17. Generally this calculation should give a good estimate for κ_L when all of the phonons are completely scattered, but here κ falls significantly below κ_{min} over a wide temperature range.

The ultralow κ at high temperatures is probably associated with the remarkable anharmonicity of Cu atoms as reflected by the large Grüneisen parameter,[17,19] but till now no substantiated model has been proposed concerning the exact action mechanism. Here we just present possible mechanisms and evaluate their rationality. According to Qiu *et al.*,[19] Cu atoms are dynamically disordered at low temperatures; they are weakly bonded to the rest of the lattice and can easily oscillate along z-direction with a large vibrational amplitude and can even transit to nearby sites, showing a "partial-liquid-like" behavior, partly blocking the heat transport. At high temperatures, apart from the dynamical disorder, structural disorder occurs as shown by the high-temperature XRD results and also suppresses heat transport.[23] Although it has been argued above that free flow of Cu atoms like that in $Cu_{2-x}Se$ seems impossible in Cu_3SbSe_3, the existence of dynamical and structural disorder is still reasonable, which may suppress phonon modes propagation to some extent (even though not as large as that in $Cu_{2-x}Se$). In addition, the breakthrough of κ_{min} could also be related to lattice softening associated with the order-disorder transition, which is the case of Zn_4Sb_3 (ref. 33) that showed a very similar behavior with Cu_3SbSe_3.

For semiconductors, the band gap is one of the key parameters that significantly affect electrical, optical and even thermal transport properties. In the field of thermoelectricity, a moderate band gap is often desired, since a very small band gap usually brings about excitation of minority carriers at relatively low temperatures, while poor electrical conductivity is often expected for materials with a very large band gap. Cu_3SbSe_3 has been found to be an indirect-gap semiconductor by band structure calculation, but the calculated gap varies significantly from 0.5 to 1.7 eV in previous reports depending on the different calculation methods.[20,24,26] In addition, few

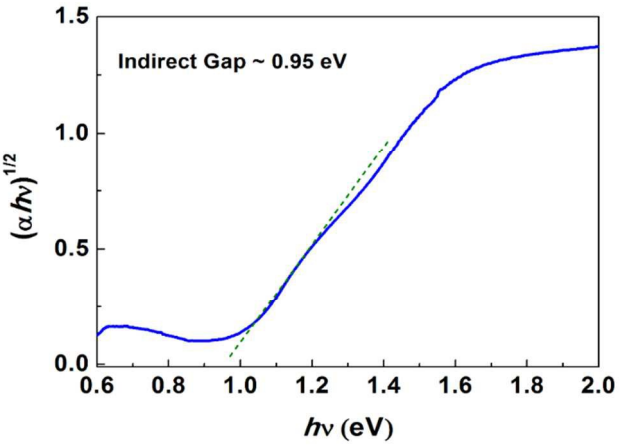

Fig. 4 Indirect band gap by optical absorption edge measurements of Cu_3SbSe_3.

experimental results are available. Here in this work, we determined the indirect gap of this material by using the optical absorption edge measurement, and the result is shown in Fig. 4. A clear absorption edge is observed and the gap was found to be 0.95 eV that is relatively large for TE materials, suggesting nondegenerate behavior in electrical transport which will be confirmed by the following results.

Fig. 5 demonstrates the temperature dependence of electrical resistivity and Seebeck coefficient. ρ is large around room temperature, ranging from 1 to 10 Ωcm depending on the fabrication method and decreases with T, finally converging to about 0.2 Ωcm at 650 K. In addition, an upturn of resistivity is seen around the transition. For all the samples, Seebeck coefficient is large and positive. The results of ρ and S indicate intrinsically p-type nondegenerate behavior in Cu_3SbSe_3, which is in agreement with the relatively large band gap.

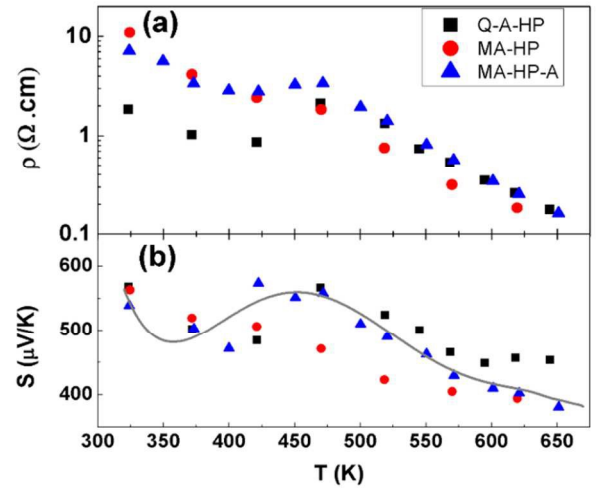

Fig. 5 Temperature dependence of (a) ρ and (b) S for Cu_3SbSe_3. The solid curve in (b) is added to guide the eyes

For a better understanding of the electrical transport, an insight is given concerning the carrier concentration and mobility. As shown in Fig. 6 (a), n_H ranges from 10^{16} to 10^{17} cm^{-3} at room temperature and keeps increasing with T to 10^{19} cm^{-3} around 500 K, again indicating nondegenerate behavior that is typical for undoped intrinsic semiconductors with a large band gap; with increased temperature, more electrons/holes are activated and become free carriers. μ_H at room temperature is 10-20 cm^2/Vs and decreases to <1 cm^2/Vs at 500 K [Fig. 6 (b)]. A dip is observed in μ_H around the transition point, explaining the upturn of ρ. These findings here on electrical transport in Cu_3SbSe_3 are in sharp contrast to previous studies where typical features of semimetals or degenerate semiconductors were demonstrated, being characterized by a high carrier concentration of 10^{19}-10^{20} cm^{-3}, as well as small S and ρ values which increase with T.[24,25] It is usually not expected that a compound with a large band gap about 1 eV could behave like semimetals. If these contradictive findings are not subjected to measurement problems, compositional deviation and unintentional doping effects brought by fabrication should be carefully evaluated. Here hot pressing and annealing were employed to reduce the amount of crystal defects. Samples prepared by different methods in this work exhibit a similarly nondegenerate behavior, thus providing a more convincing insight into the intrinsic transport properties of the compound. Compared with hot pressing, SPS (used in refs. 24 and 25) is a fast sintering technique that usually yields samples in a non-equilibrium state with large amount of crystal defects that may cause self-doping effect and dramatically change the transport properties. Although the exact type and amount of the defects in compounds from previous studies[24,25] are still unclear, a possibility cannot be ruled out that cation vacancies, probably Cu vacancies, accompanied by the generation of additive hole carriers may be responsible for the metallic behaviour with a high hole concentration in Cu_3SbSe_3 samples from the earlier reports.

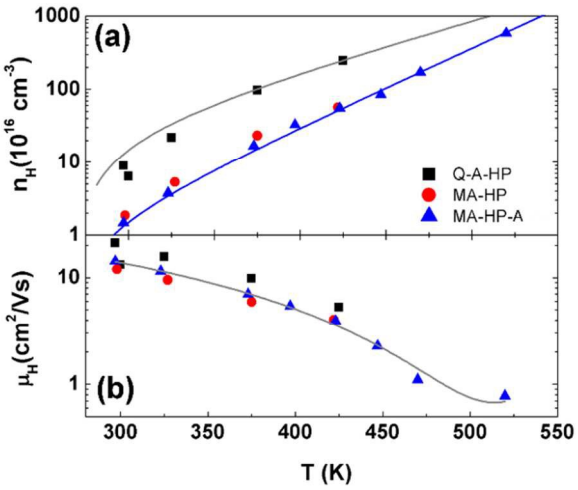

Fig. 6 (a) n_H and (b) μ_H as functions of temperature. Solid lines are added to guide the eyes.

The calculated power factor (PF) reaches 100±10 μW/mK^2 at 650 K as indicated in Fig. 7 (a). The low PF of Cu_3SbSe_3 is mainly caused by the high electrical resistivity, *i.e.* the small carrier concentration and low carrier mobility. The carrier concentration may be tuned by proper doping, but it is difficult to enhance the mobility. Here we present a brief discussion on the origin of low mobility of Cu_3SbSe_3 and evaluate some physical parameters of this material with Cu_3SbSe_4 as a comparison.

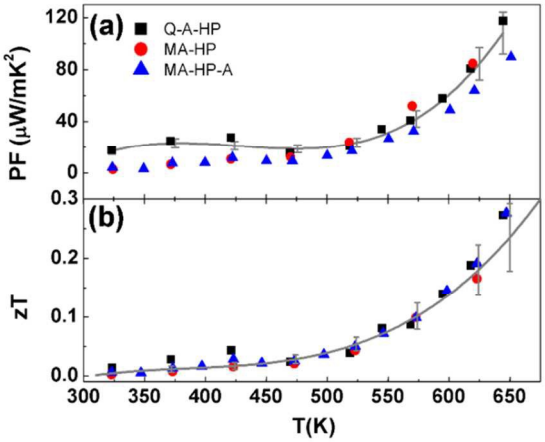

Fig. 7 (a) Power factor and (b) *zT* as functions of temperature for Cu_3SbSe_3 with estimated uncertainties of 15 % and 20%, respectively. Solid lines are added to guide the eyes.

It is known that low mobility is often caused by large effective mass through Eq. (3) under single parabolic band (SPB) model[34] with the assumption of acoustic phonon scattering being dominant:

$$\mu_H = \frac{\pi e\hbar^4 d v_l^2}{2\sqrt{2} m_b^{*3/2} m_I^* (k_B T)^{3/2} \Xi^2} \frac{F_{-1/2}(\eta)}{F_0(\eta)}, \quad (3)$$

where m_b^* and m_I^* are the band and inert effective mass, respectively; Ξ, η and F_n are the deformation potential, chemical potential and Fermi integrals, respectively.[22,35] m_b^* and m_I^* are related to the effective mass components along principal directions m_j^* (j=1, 2, 3) *via* $m_I^{*-1}=1/3\ (m_1^{*-1}+m_2^{*-1}+m_3^{*-1})$, and $m_b^*=(m_1^* m_2^* m_3^*)^{1/3}$.(ref. 36) The density-of-state effective mass m_d^* is determined by both the band effective mass and the band degeneracy N_V *via* $m_d^*= m_b^* N_V^{2/3}$ (refs. 36 and 37). For Cu_3SbSe_3, m_b^*, m_I^* and m_d^* were calculated using the value of m_j^* (j=1, 2, 3) given in ref. 26. For Cu_3SbSe_4, m_d^* was taken from refs. 22 and 38 while m_b^* was calculated and m_I^* was assumed equal to m_b^*. Some of the key physical parameters relevant are shown in Table 2 for Cu_3SbSe_3 and Cu_3SbSe_4.

Table 2 The mobility together with other physical parameters for Cu_3SbSe_3 and Cu_3SbSe_4 around room temperature. [a]Band degeneracies (N_V) are indicated from calculation of refs. 20 and 21. [b]Values of v_l are taken from ref. 17. [c]Parameters of Cu_3SbSe_4 are taken from refs. 22 and 38.

System	Cu_3SbSe_3	Cu_3SbSe_4[c]
Space group	Pnma	I-42m
E_g (eV)	Indirect 0.95	Direct 0.29
N_V[a]	1	3
$m_d^*(m_e)$	0.6	1.1-1.5
$m_b^*(m_e)$	0.6	0.5-0.7
$m_I^*(m_e)$	0.5	0.5-0.7
Ξ(eV)	32±5	15 ± 0.5
$d\,v_l^2$ (GPa)[b]	57	73
μ_H(cm²/Vs)	12-21	110

It is seen that m_b^* and m_I^* of Cu_3SbSe_3 are relatively large and comparable to those of Cu_3SbSe_4, which, however, has a much larger mobility. In addition to the effective mass, mobility is also governed by the deformation potential, Ξ, which was fitted to be about 32 eV for Cu_3SbSe_3, approximately twice that of Cu_3SbSe_4, indicating strong coupling between carriers and phonons. In addition, it has been well recognized that band convergence or multi-valley effect (existence or creation of large N_V) can benefit high TE performance since a larger N_V leads to a larger carrier concentration when with a constant Seebeck coefficient. This fact has been proved in almost all high-performance TE materials, such as lead chalcogenides,[37,39] Bi_2Te_3 (ref. 40), Half-Heusler compounds,[41] Mg_2Si (ref. 42) and chalcopyrite-like compounds.[43,44] However, it is not the case of Cu_3SbSe_3 where N_V is only 1, originating from the low symmetry in crystal structure. When considering the thermoelectric quality factor B, defined as[35]

$$B = \frac{2k_B^2\hbar}{3\pi} \frac{d v_l^2 N_V}{m_I^* \Xi^2 \kappa_L} T, \quad (4)$$

it comes to the realization that the singe and heavy band character, and large deformation potential in Cu_3SbSe_3 are probably the underlying factors causing the inferior TE performance that could hardly be compensated by the low lattice thermal conductivity.

zT as a function of temperature is depicted in Fig. 7 (b). The maximum value of 0.25 was obtained at 650 K in both Q-A-HP and MA-HP-A. *zT* is expected to continue rising when *T* goes higher, but the low melting temperature (~730 K by DSC) limits the operation at high temperatures. Although *zT* value in this work is much higher than previously reported ones (<0.1),[24,25] it is remarkably lower than that of Cu_3SbSe_4, let alone those state-of-the-art TE materials. Attempts have been made to increase the carrier concentration by doping Ge on Sb site and substituting Te for Se *via* MA and HP but failed. Bi-substitution for Sb was found to successfully increase the carrier concentration and electrical conductivity at room temperature, but no enhancement of *PF* was obtained at high temperatures. Considering the large band gap, the single and heavy band character, large deformation potential, possible liquid-like behavior as well as the order-disorder transition, Cu_3SbSe_3, even with an ultralow thermal conductivity, may not be as competitive as Cu_3SbSe_4 in TE performance.

Conclusions

In summary, Cu_3SbSe_3 was found to possess an ultralow thermal conductivity over a wide temperature range. Cu atoms in Cu_3SbSe_3 were considered much less mobile than in $Cu_{2-x}Se$ but still dynamically and structurally disordered to a great extent, and their behavior was thought to partly suppress the heat transport. Cu_3SbSe_3 with a large band gap of 0.95 eV demonstrated a nondegenerate character, in marked contrast to previous studies. Maximum *zT* of ~0.25 was obtained at 650 K for Cu_3SbSe_3 that may not be so competitive as Cu_3SbSe_4 in thermoelectric performance due to the single and relatively heavy valence band, large band gap, strong electron-phonon coupling, possible liquid-like behavior and the phase transition of the former. These findings in this work will advance the understanding of thermoelectric transport properties of Cu_3SbSe_3 and other multinary selenides.

Acknowledgements

This work is supported by National Natural Science Foundation (Nos. 51172121, 11474176) and the 973 Program (Grant No. 2013CB632503).

Notes and references

State Key Laboratory of New Ceramics and Fine Processing, School of Materials Science and Engineering, Tsinghua University, Beijing 100084, China.

**E-mail: jingfeng@mail.tsinghua.edu.cn; Fax: +86-10-62771160; Tel: +86-10-62784845*

† Electronic Supplementary Information (ESI) available: Repeated measurements of thermoelectric properties of the samples.

1 G. J. Snyder and E. S. Toberer, *Nat. Mater.*, 2008, **7**, 105-114.
2 L. E. Bell, *Science*, 2008, **321**, 1457-1461.
3 M. Zebarjadi, K. Esfarjani, M. S. Dresselhaus, Z. F. Ren and G. Chen, *Energy Environ. Sci.*, 2012, **5**, 5147-5162.
4 J.-F. Li, W.-S. Liu, L.-D. Zhao and M. Zhou, *NPG Asia Mater.*, 2010, **2**, 152-158.
5 L.-D. Zhao, V. P. Dravid and M. G. Kanatzidis, *Energy Environ. Sci.*, 2014, **7**, 251-268.
6 J. Yang, H.-L. Yip and A. K.-Y. Jen, *Adv. Energy Mater.*, 2013, **3**, 549-565.
7 P. Sundarraj, D. Maity, S. S. Roy and R. A. Taylor, *RSC Adv.*, 2014, **4**, 46860-46874.
8 L. D. Zhao, D. Berardan, Y. L. Pei, C. Byl, L. Pinsard-Gaudart and N. Dragoe, *Appl. Phys. Lett.*, 2010, **97**, 092118.
9 J. Sui, J. Li, J. He, Y.-L. Pei, D. Berardan, H. Wu, N. Dragoe, W. Cai and L.-D. Zhao, *Energy Environ. Sci.*, 2013, **6**, 2916-2920.
10 H. Liu, X. Shi, F. Xu, L. Zhang, W. Zhang, L. Chen, Q. Li, C. Uher, T. Day and G. J. Snyder, *Nat. Mater.*, 2012, **11**, 422-425.
11 D. Li, X. Y. Qin, Y. F. Liu, C. J. Song, L. Wang, J. Zhang, H. X. Xin, G. L. Guo, T. H. Zou, G. L. Sun, B. J. Ren and X. G. Zhu, *RSC Adv.*, 2014, **4**, 8638-8644.
12 L.-D. Zhao, S.-H. Lo, Y. Zhang, H. Sun, G. Tan, C. Uher, C. Wolverton, V. P. Dravid and M. G. Kanatzidis, *Nature*, 2014, **508**, 373-377.
13 C.-L. Chen, H. Wang, Y.-Y. Chen, T. Day and G. J. Snyder, *J. Mater. Chem. A*, 2014, **2**, 11171-11176
14 E. J. Skoug, J. D. Cain and D. T. Morelli, *Appl. Phys. Lett.*, 2011, **98**, 261911.
15 D. Li, R. Li, X.-Y. Qin, C.-J. Song, H.-X. Xin, L. Wang, J. Zhang, G.-L. Guo, T.-H. Zou, Y.-F. Liu and X.-G. Zhu, *Dalton Trans.*, 2014, **43**, 1888-1896.
16 Y. Zhang, V. Ozoliņš, D. Morelli and C. Wolverton, *Chem. Mater.*, 2014, **26**, 3427–3435.
17 Y. Zhang, E. Skoug, J. Cain, V. Ozoliņš, D. Morelli and C. Wolverton, *Phys. Rev. B: Condens. Matter Mater. Phys.*, 2012, **85**, 054306.
18 E. J. Skoug and D. T. Morelli, *Phys. Rev. Lett.*, 2011, **107**, 235901.
19 W. Qiu, L. Xi, P. Wei, X. Ke, J. Yang and W. Zhang, *Proc. Natl. Acad. Sci. U. S. A.*, 2014, **111**, 15031-15035.
20 D. Do, V. Ozolins, S. D. Mahanti, M.-S. Lee, Y. Zhang and C. Wolverton, *J. Phys.: Condens. Matter*, 2012, **24**, 415502.
21 D. T. Do and S. D. Manhanti, *J. Alloys Compd.*, 2015, **625**, 346-354.
22 T.-R. Wei, H. Wang, Z. M. Gibbs, C.-F. Wu, G. J. Snyder and J.-F. Li, *J. Mater. Chem. A*, 2014, **2**, 13527-13533.
23 M. Kirkham, P. Majsztrik, E. Skoug, D. Morelli, H. Wang, W. D. Porter, E. A. Payzant and E. Lara-Curzio, *J. Mater. Res.*, 2011, **26**, 2001-2005.
24 K. Tyagi, B. Gahtori, S. Bathula, A. K. Srivastava, A. K. Shukla, S. Auluck and A. Dhar, *J. Mater. Chem. A*, 2014, **2**, 15829-15835.
25 K. Tyagi, B. Gahtori, S. Bathula, V. Toutam, S. Sharma, N. K. Singh and A. Dhar, *Appl. Phys. Lett.*, 2014, **105**, 261902.
26 A. B. Kehoe, D. J. Temple, G. W. Watson and D. O. Scanlon, *Phys. Chem. Chem. Phys.*, 2013, **15**, 15477-15484.
27 A. Pfitzner, *Z. Anorg. Allg. Chem.*, 1995, **621**, 685-688.
28 K. Samanta, N. Gupta, H. Kaur, L. Sharma, S. Dogra Pandey, J. Singh, T. D. Senguttuvan, N. Dilawar Sharma and A. K. Bandyopadhyay, *Mater. Chem. Phys.*, 2015, **151**, 99-104.
29 D. G. Cahill and R. C. Pohl, *Phys. Rev. B: Condens. Matter Mater. Phys.*, 1987, **35**, 4067-4073.
30 E. S. Toberer, L. L. Baranowski and C. Dames, *Annu. Rev. Mater. Res.*, 2012, **42**, 179-209.
31 K. W. Schlichting, N. P. Padture and P. G. Klemens, *J. Mater. Sci.*, 2001, **36**, 3003-3010.
32 D. G. Cahill, S. K. Watson and R. O. Pohl, *Phys. Rev. B: Condens. Matter Mater. Phys.*, 1992, **46**, 6131-6140.
33 S. Bhattacharya, R. P. Hermann, V. Keppens, T. M. Tritt and G. J. Snyder, *Phys. Rev. B: Condens. Matter Mater. Phys.*, 2006, **74**, 134108.
34 A. F. May and G. J. Snyder, in *THERMOELECTRICS AND ITS ENERGY HARVESTING*, ed. D. M. Rowe, CRC Press, Boca Raton, 2012, ch. 11.
35 H. Wang, Y. Pei, A. D. LaLonde and G. J. Snyder, in *Thermoelectric Nanomaterials: Materials Design and Applications*, eds. K. Koumoto and T. Mori, Springer, Heidelberg, 2013, pp. 3-32.
36 C. M. Bhandari, in *CRC Handbook of Thermoelectrics*, ed. D. M. Rowe, CRC Press, Boca Raton, 1995, pp. 27-42.
37 Y. Pei, X. Shi, A. LaLonde, H. Wang, L. Chen and G. J. Snyder, *Nature*, 2011, **473**, 66-69.
38 T.-R. Wei, F. Li and J.-F. Li, *J. Electron. Mater.*, 2014, **43**, 2229-2238.
39 H. Wang, Z. M. Gibbs, Y. Takagiwa and G. J. Snyder, *Energy Environ. Sci.*, 2014, **7**, 804-811.
40 G. S. Nolas, J. Sharp and H. J. Goldsmid, *Thermoelectrics: Basic Principles and New Materials Developments*, Springer, Berlin, 2001.
41 C. Fu, T. Zhu, Y. Pei, H. Xie, H. Wang, G. J. Snyder, Y. Liu, Y. Liu and X. Zhao, *Adv. Energy Mater.*, 2014, **4**, 1400600.
42 W. Liu, X. Tan, K. Yin, H. Liu, X. Tang, J. Shi, Q. Zhang and C. Uher, *Phys. Rev. Lett.*, 2012, **108**, 166601.
43 J. Zhang, R. Liu, N. Cheng, Y. Zhang, J. Yang, C. Uher, X. Shi, L. Chen and W. Zhang, *Adv. Mater.*, 2014, 26, 3848-3853.
44 D. Zou, G. Nie, Y. Li, Y. Xu, J. Lin, H. Zheng and J. Li, *RSC Adv.*, 2015, 5, 24908-24914.

